International Journal of Fatigue 117 (2018) 13–20

Contents lists available at ScienceDirect

International Journal of Fatigue

journal homepage: www.elsevier.com/locate/ijfatigue

# Interaction of hot corrosion fatigue and load dwell periods on a nickel-base single crystal superalloy

L. Brooking*, S. Gray, J. Sumner, J.R. Nicholls, N.J. Simms

*Cranfield University, College Road, Cranfield MK43 0AL, UK*

ARTICLE INFO

*Keywords:*
Hot corrosion
Fatigue dwell period
Single crystal superalloy

ABSTRACT

The effects of type II hot corrosion on the fatigue resistance of turbine blade superalloys is of growing interest as gas turbine (GT) original equipment manufacturers (OEMs) strive to optimise the operational efficiencies and versatilities of GT systems. Hot corrosion fatigue has been observed in the under platform regions of first stage GT blades, this location is subject to both relatively high principal stresses and stress gradients, combined with temperatures up to those associated with type II hot corrosion (500–700 °C). The effect of the deposition flux of corrosive salt species and the tensile stress dwell period on the fatigue performance and resultant crack morphologies of single crystal (SC) superalloy CMSX-4 has been studied at 550 °C. Deposit recoat methodologies were applied to specimens that were cyclically fatigued with a load-controlled trapezoidal waveform. It was observed that introducing a longer dwell period increased the number of {1 0 0} crack initiations and reduced the fatigue life (load cycles to failure). Optical and SEM microscopy and EDX techniques were used to examine specimen fractography, and mechanisms of crack advance and propagation discussed.

## 1. Introduction

Gas turbines (GTs) are used for a range of power generation applications; some of the more common being industrial power generation and aviation engines. With GTs relevance to the future of energy and aerospace industries looking to remain high [1], and demand for GTs to generate sustainable clean and efficient power being significant [1–3], GT original equipment manufacturers (OEMs) are constantly striving to optimise operation and efficiencies. One of the key limiting factors effecting the power density and thermal efficiencies that can be achieved by GTs is the operational gas temperatures reached in the turbine section of the engine. These gas temperatures are largely limited by the material capabilities in the following areas; high temperature oxidation/corrosion performance, and high temperature mechanical performance such as creep and fatigue [4]. Often blade cooling is used in first stage turbines in order to reduce the blade temperatures and improve the mechanical properties, however the increasing temperatures can result in the extended effect of hot corrosion. In addition to increasing temperatures the low cycle fatigue (LCF) duty cycles GTs are subjected to can also be intensified as a result of increased multi start up and shut down procedures. This can be as a result of increased renewables and peak loads on the energy grid in the case of industrial GTs, and increased short haul flights in the case of aviation engines. These combined factors provide the motivation for conducting combined hot corrosion fatigue testing.

Due to the importance of the high temperature material properties and degradation models for GT component design, there is a large amount of research available and a good understanding of them [5–7]. However, whilst it has been observed [8], the interactions and mechanisms generated as a result of combined hot corrosion and mechanical fatigue is not currently a heavily researched area and as such there is a limited understanding of these interactions. As a result, combined material degradation mechanisms not predicted by current design life methods have resulted from simultaneous hot corrosion and mechanical fatigue [9]. Type II hot corrosion has been reported to both assist crack initiation due to corrosion pitting, and accelerate fatigue crack propagation [10]. The work presented in this paper focuses on type II hot corrosion and fatigue interactions, and studies the effect of extended dwell periods on fatigue life in the single crystal turbine blade alloy CMSX-4. Dwell effects on hot corrosion fatigue have been studied in a disk alloy [11], it was found that increased dwell resulted in a decrease in fatigue life, which was attributed to time dependant mechanisms such as crack tip oxidation. This paper further hypothesises that this effect could in part be due to additional crack growth occurring in a period of static load, such as a fatigue dwell period. This hypothesis is informed by previous research showing that cracks can

* Corresponding author.
*E-mail address:* l.b.brooking@cranfield.ac.uk (L. Brooking).

https://doi.org/10.1016/j.ijfatigue.2018.07.029
Received 14 June 2018; Received in revised form 20 July 2018; Accepted 24 July 2018
Available online 25 July 2018

**Table 1**
Composition of CMSX-4 (wt%), Ni Bal.

| Cr | W | Co | Mo | Al | Ti | Ta | Re | Hf |
|---|---|---|---|---|---|---|---|---|
| 6.5 | 6.0 | 9.6 | 0.6 | 5.6 | 1.0 | 6.5 | 3..0 | 0.1 |

initiate and propagate under static loads when combined with type II hot corrosion [12,13]. Dwell periods were introduced using a trapezoidal waveform, on the first stage turbine blade material, single crystal nickel based superalloy CMSX-4 (Table 1).

Type II hot corrosion is induced through salt deposition combined with a regular supply of $SO_x$ [14]. Salt species typically deposit on the surface of GT components, forming low melting point mixtures with alloying elements. This mechanism commonly produce corrosion products rich in $CoSO_4$ and $NiSO_4$ for nickel-based superalloys such as CMSX-4 [15,16]. In gas turbines, sulphur can be introduced into the system through both fuel and air contaminants. However salt species are normally introduced into the turbine via the air intake; this can be in the form of particulate or liquid matter, which can then deposit onto turbine components via two mechanisms. The salt species can either be vaporised or sublimated in the combustion process, and then condense onto turbine components, this is commonly referred to as vapour deposition [17]. Additionally, salt species can deposit due to particles sticking onto turbine components; resulting in a build-up of deposit [18]. A combination of these mechanisms can occur depending on the temperatures and pressures at certain locations in the turbine, a model for similar deposition mechanisms in pulverised coal boilers was proposed by Tomeczek et al [19].

The effect of the deposition flux of corrosive salts on the fatigue resistance and resulting crack morphologies of single crystal (SC) superalloy CMSX-4 was previously experimentally studied at 550 °C [13]. It was found that an increase in the deposition flux had a detrimental effect on the fatigue resistance of CMSX-4. Additionally, the increase in flux generated a shift in the crack propagation plane from the conventional {1 1 1} slip systems [20,21], to a orthogonal {1 0 0} propagation. This was observed in plane cylindrical specimens with no stress concentration. This behaviour was associated with the orthogonal corrosion attack and embrittlement of the primary gamma-prime strengthening phase at the crack tip.

The stability of a crack under fatigue loading can be simplistically assessed through the use of linear elastic fracture mechanics (LEFM) [22]. In order for fatigue crack propagation to occur the stress intensity has to overcome the fatigue threshold value ($K_{TH}$). For CMSX-4 at a temperature of 550 °C this has been determined to be in the range of 15 MPa $\sqrt{m}$ [23].

Conventional fatigue is defined as occurring in three stages defined as follows [24,25]. Stage 1 is defined as crack nucleation and initiation and is arguably the least well understood and most heavily researched area of fatigue. Crack nucleation and initiation is thought to occur due to cyclic loading causing shear slip and resulting in the generation and accumulation of micro pours which initiate a fatigue crack. Stage 2 is the propagation stage which is arguably the most well understood stage and can be simplistically modelled using Paris law and fracture mechanics. Fatigue crack propagation is thought to occur due to cyclic loading generating plastic slip which results in dislocation emissions ahead of the crack tip. Stage 3 is the final rupture stage where the reduction in cross-section leads to mechanical over load.

## 2. Methodology

### 2.1. Experimental methodology

Accelerated type II hot corrosion conditions were generated by depositing an 80/20 mol% mix of $Na_2SO_4/K_2SO_4$ over 100 h intervals in order to maintain a consistent deposition flux. A test gas of 300 ppm $SO_x$ and air was passed through the test chamber to maintain a partial pressure of $SO_x$. Specimens were subjected to a temperature of 550 °C via radiated heat from a sheath which was in turn induction heated (Fig. 1). Specimens were pre-corroded for 500 h with either a 1.25 or 5 μg/cm$^2$/h flux.

The specimens used were cylindrical plain specimens oriented in the [0 0 1] direction, meaning the [0 0 1] axis is aligned to the length of the cylindrical gauge length of the specimen to within a tolerance of ± 20°. Therefore the crystallographic groups for directions and planes can be determined from this known [0 0 1] axis alignment. The cylindrical gauge length of 6 mm diameter generates a uniaxial stress state within the specimen.

The procedure used for fatigue testing is outlined in Fig. 2 where all specimens were exposed for 500 h of pre corrosion in order to

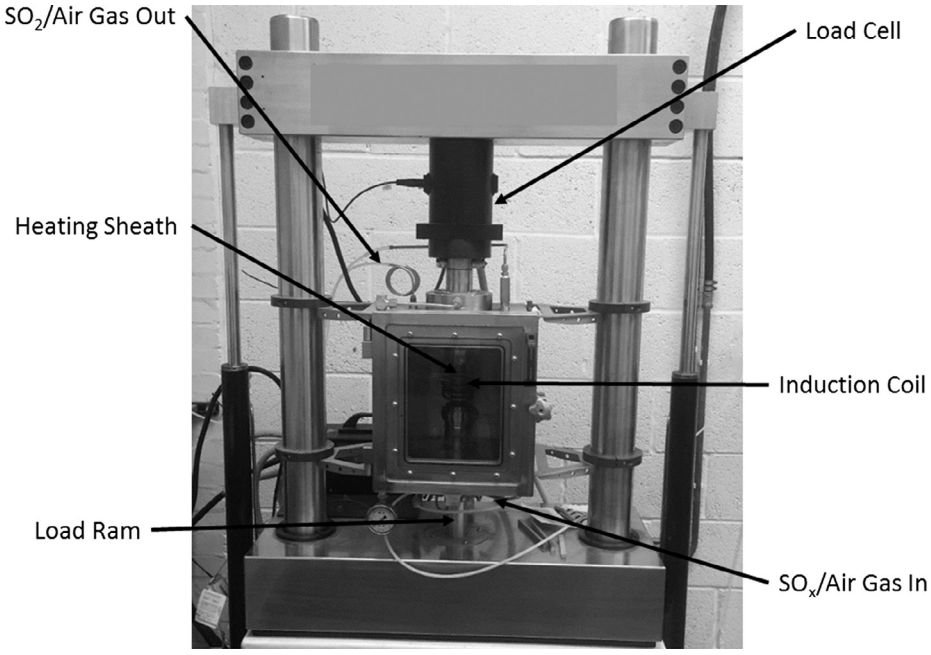


**Fig. 1.** Cranfield load controlled corrosion fatigue rig.

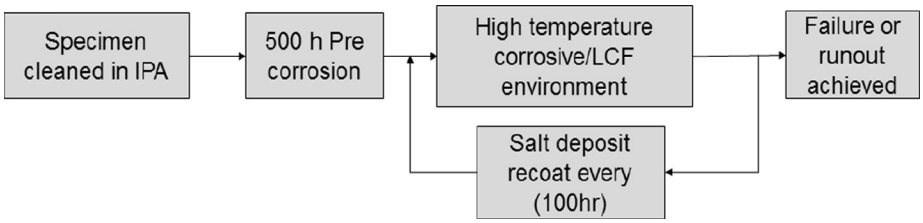


**Fig. 2.** Flow chart outlining the type II hot corrosion fatigue testing procedure.

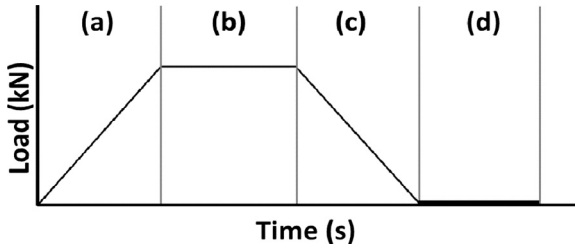


**Fig. 3.** Trapezoidal load wave form: (a) ramp up period, (b) maximum stress dwell period, (c) ramp down period, (d) minimum load dwell period.

accelerate the corrosive environment. Fatigue specimens were subjected to a fully tensile un-reversed (R = 0) trapezoidal load controlled waveform (Fig. 3). The waveforms used were 1-1-1-1 s and 1-60-1-1 s. Fatigue cycles were controlled through a servo hydraulic load feedback control loop and S-N curves were plotted for stress levels between 700 and 850 MPa.

### 2.2. Analytical methodology

Post testing specimens were examined using scanning electron microscopy (SEM) and characterised with energy dispersive X-rays (EDX). Both Phillips FEI XL-30 and JEOL 7800F systems were used to analyse fracture surfaces and cross-sections. Cross-sections were mounted in a 50:50 mixture of epoxy resin and ballotoni (40–70 μm diameter glass beads), then polished using oil lubricant to preserve the corrosion products.

Analysis of the banding observed on fracture faces was conducted using Image-J [26] to assess crack propagation paths and environmentally induced banding spacing.

## 3. Results

### 3.1. Experimental results

For the 5 μg/cm$^2$/h deposition flux curves a reduction in fatigue life of up to four times was observed with the introduction of a 60 s dwell period (Fig. 4). However as the gradient of the 60 s dwell curve is shallower than that of the 1-1-1-1 curve. It should be noted that dwell has a detrimental effect on fatigue life, and the data suggests that this is more marked at higher stresses.

To provide an additional comparison, the 1.25 and 5 μg/cm$^2$/h deposition flux curves for 1-1-1-1 cycle has been included, as previously presented in [13]. It can be seen that the relative effect of dwell from 1-1-1-1 to 1-60-1-1 is significantly greater than the increased flux from 1.25 to 5 μg/cm$^2$/h.

When considering the time to failure, due to the increased cycle length of the 1-60-1-1 waveform compared with that of the 1-1-1-1, the longer dwell has the impact of increasing the time to failure by up to two times (Fig. 5). Similarly the shallower gradient of the 60 s dwell curve suggests that longer dwell specimens take a relatively greater time to fail at lower stresses. However due to the length of 60 s dwell tests, testing with lower stresses achieved a runout defined as over 200 h of testing.

### 3.2. Fractographic analysis

Optical images of fracture faces on 60 s dwell samples show multiple {1 0 0} crack initiations and subsequent propagation in the form of semi elliptical thumbnails (Fig. 6). After a period of {1 0 0} propagation the cracks transition to {1 1 1} propagation. During this rapid {1 1 1} mechanical crack growth driven by fatigue cycles, fatigue striations were observed on the fracture face/facets. In relation to the presented analysis, striations were defined as rigged demarcation formed as a result of fatigue crack propagation and generated predominantly on {1 1 1} facets on the fracture faces examined. Environmental banding were defined as corrosion/oxidation demarcation generated predominantly on {1 0 0} planes on the fracture faces examined.

Energy dispersive X-ray (EDX) analysis performed on an SEM, of environmental banding on a fracture face (Fig. 7) is presented in Table 2. It can be see that the spectrum locations 1 and 2, taken in the oxide banding contain Ni, O and S, suggesting they are a corrosion product of type II hot corrosion [15,16]. Spectrum location 1 taken in the γ/γ′ microstructure contains a comparable wt% of elements as to the substrate alloy CMSX-4, presented in Table 1.

SEM fracture face images of a 750 MPa, 1-1-1-1 loaded specimen are shown in Fig. 8. Closely spaced environmentally induced oxidation/corrosion banding can be seen on the {1 0 0} fracture face. Additionally fatigue striations can be seen on the same sample later in the crack propagation path, these are generated on a {1 1 1} fracture face and are most likely produced in the cycles just prior to mechanical overload, when a relatively high ΔK is present at the crack tip. Similar oxidation banding and marking can also be seen on the fracture face of an 800 MPa, 1-1-1-1 loaded specimen presented in Fig. 9, along with build-up of corrosion product on the fracture surface.

Comparative SEM images of fracture faces from 800 to 850 MPa specimens, with a 1-60-1-1 waveform are given in Fig. 10 and Fig. 11. These images demonstrate the initial transitioning from the {1 0 0} fracture plane to {1 1 1} rooftop peaks as the fatigue threshold is exceeded. Environmental oxide/corrosion banding, and {1 1 1} fatigue striations are also visible.

It was noted that the small environmental banding spacing, such as those visible on the 1 s dwell fracture face shown in Figs. 8 and 9, were not clearly visible on 60 s dwell faces (Figs. 10 and 11). It is possible that this banding, generated during fatigue crack initiation, has subsequently been covered up by corrosion product in the 60 s dwell test due to the longer durations specimens were exposed to resulting in higher levels of corrosion on the fractured face.

A summary of the number of initiation sites visible over the fracture face area, and of the environmentally induced oxidation/corrosion banding markings are presented in Table 3. These values are estimations taken from measurements of optical and SEM images.

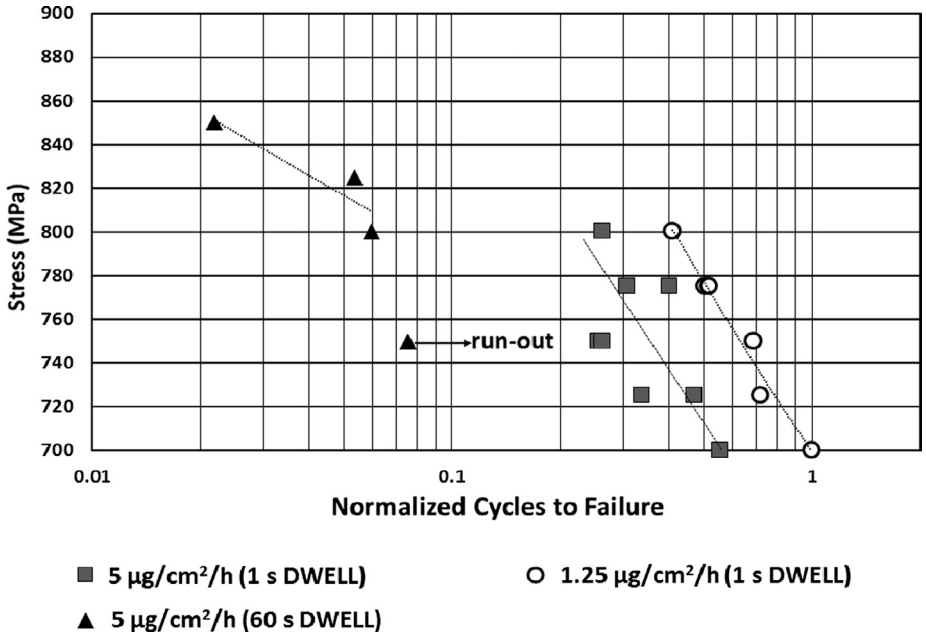


**Fig. 4.** Normalised cycles to failure S-N curve, 1 s dwell curves are previously presented in [13].

## 4. Discussion

Dwell had a significant impact on reducing the fatigue life when acting in combination with type II hot corrosion. There are several plausible mechanisms as to why dwell has this effect. One is that holding the crack open for prolonged dwell periods allows the corrosive contaminates to diffuse to the crack tip. This results in increased oxidation around the crack tip, enabling the fatigue/cracking mechanism to continue to propagate. A second mechanism is based upon previous research that demonstrated a combined static stress and type II hot corrosion cracking [12,13]. It is therefore plausible that under similar conditions crack propagation can occur during static load dwell periods as well as due to conventional fatigue cycling. This static crack propagation would aid the nucleation and initiation of a fatigue crack. It is also possible however that a combination of enhanced diffusion of corrosive species to the crack tip and static load crack propagation is also occurring and accelerating crack propagation under longer dwell exposures.

It was observed that, whilst dwell reduced the cycles to failure, it took a relatively longer test duration for 60 s dwell specimens to fail. This can also be explained by considering the dwell as accelerating crack initiation and being dependant on exposure time at maximum stress, however when the fatigue threshold is exceeded, the fatigue frequency and $\Delta K$ become the dominate factors behind crack propagation. With service conditions generating much longer max stress dwell periods in combination with high cycle fatigue (HCF) and low

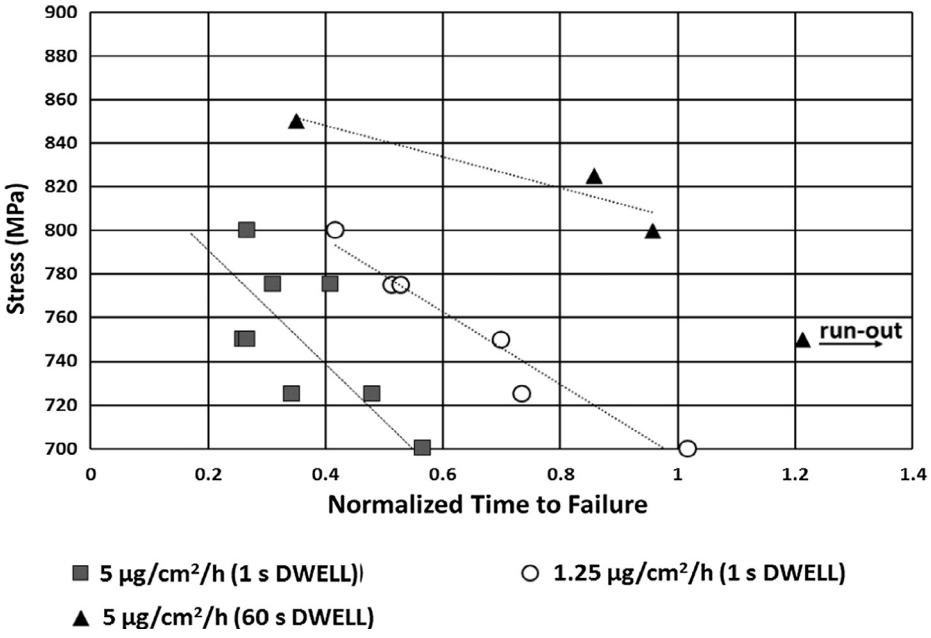


**Fig. 5.** Normalised time to failure.

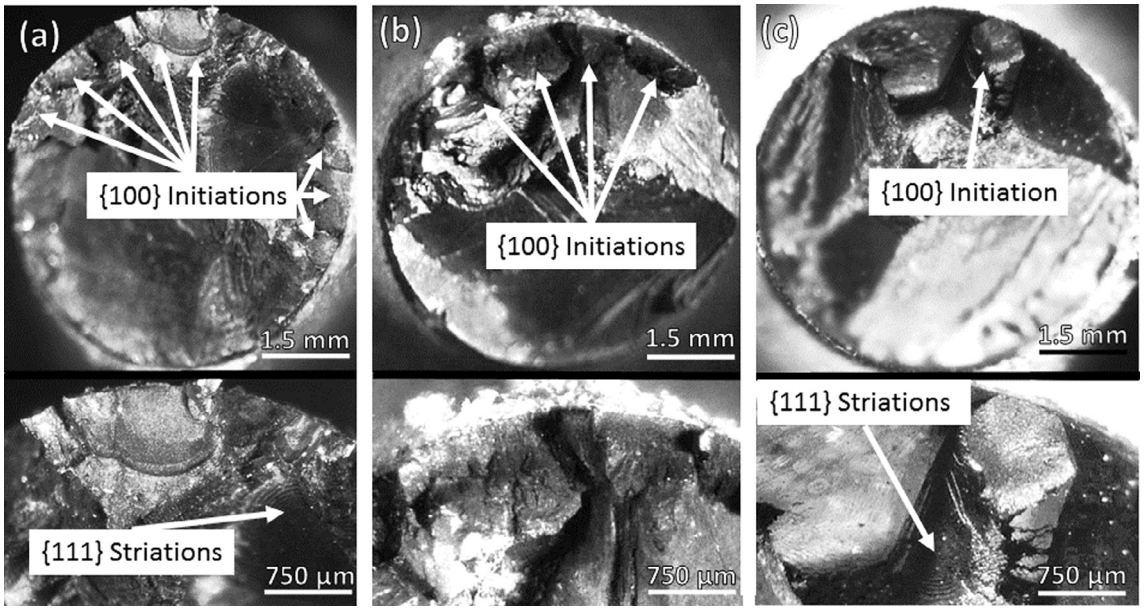


**Fig. 6.** Optical microscope images of fracture surfaces (a) 800 MPa, 5 µg/cm$^2$/h deposit flux, 1-60-1-1 (b) 850 MPa, 5 µg/cm$^2$/h, 1-60-1-1 (c) 800 MPa, 5 µg/cm$^2$/h, 1-1-1-1 [13].

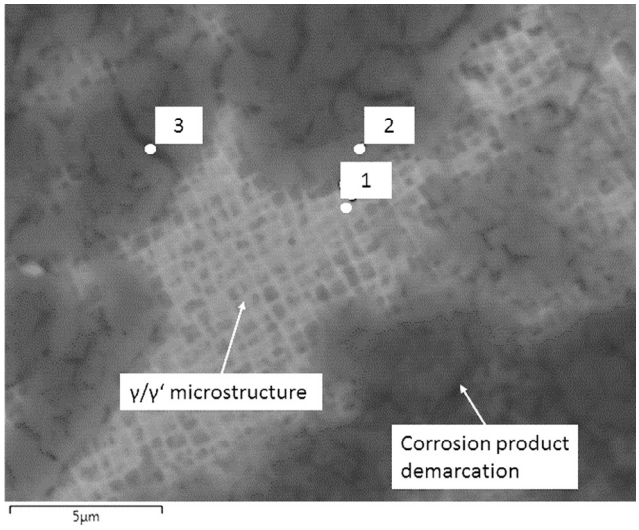


**Fig. 7.** Back scattered SEM image of environmental/corrosion banding on a {1 0 0} fracture face, EDX spectrums were taken in locations 1, 2 and 3 and are presented in Table 2.

cycle fatigue (LCF) [27], it is possible that dwell propagation could be the dominate propagation mechanism for crack initiation, and HCF/LCF for fatigue crack propagation until final fracture.

An increased number of {1 0 0} crack initiations where observed with the introduction of 60 s dwell and with lower stress dwell tests. It is proposed that there are two contributors for this. Firstly as a result of crack tip oxidation/corrosion resulting in crack tip blunting and enhanced crack initiations [28]. And secondly as a result of the static stress crack propagation associated with fatigue crack initiation, being partly independent of stress concentration/intensity.

It can be theorised from fracture face analysis that the combined type II hot corrosion fatigue cracking mechanism exhibits a stop/start behaviour during crack initiation both with 1 and 60 s dwell. This generates the environmental oxidation/corrosion banding. It is postulated that this results from a time dependant embrittlement mechanism at the crack tip causing crack arresting or abrupt changes in the propagation rate.

Measuring the spacing between environmental oxidation/corrosion banding demonstrates that the spacing can be significantly different between 1 s dwell and 60 s dwell waveform. Additionally the banding looks visibly different, with 1 s dwell leaving light surface discolorations in the γ/γ′ microstructure, whereas 60 s dwell leaves a thick scale banding on top of the γ/γ′ microstructure. This difference in resultant fracture face could be due to the early environmental banding being masked by corrosion scale on the longer 60 s dwell tests. Additionally it could be due to the dominance of static stress corrosion cracking generating larger beach mark type banding such as those scene in static stress testing [12].

The shell shaped and semi-circular markings observed in the scale on the 60 s dwell fracture faces have contours which match those of the environmental oxidation markings. And are therefore likely to be associated with crack arresting or abrupt changes in the propagation rate.

Changes in the fracture face morphology can in part be associated with the crack transitioning from stage 1 sub fatigue threshold crack initiation, to stage 2 Paris crack growth occurring above the fatigue threshold. Previously conducted finite element (FE) modelling [13]

**Table 2**
EDX analysis from spectrum locations given in Fig. 7.

| Spectrum | Ni wt% | Co wt% | Cr wt% | O wt% | W wt% | Al wt% | C wt% | S wt% | Ta wt% |
|---|---|---|---|---|---|---|---|---|---|
| 1 | 52 | 9 | 8 | 9 | 8 | 8 | 0 | 0 | 5 |
| 2 | 41 | 7 | 4 | 22 | 2 | 3 | 8 | 5 | 0 |
| 3 | 45 | 9 | 4 | 21 | 3 | 2 | 9 | 5 | 0 |

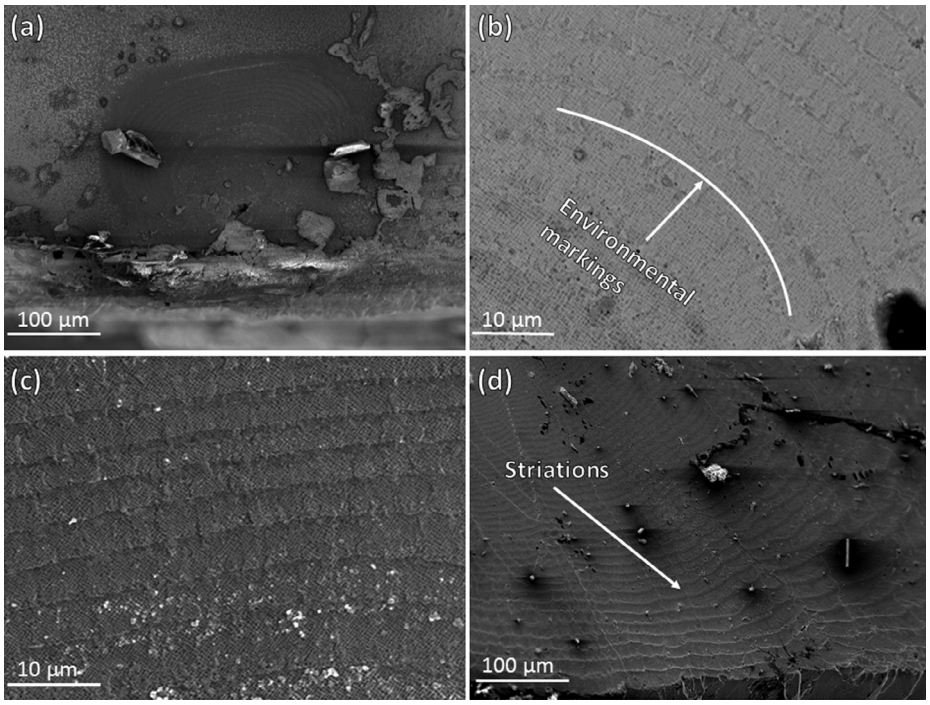


**Fig. 8.** Fracture face images of specimen exposed to 750 MPa, 1-1-1-1, 5 µg/cm$^2$/h deposit flux (a) Secondary electron (SE) image of {1 0 0} crack initiation and propagation showing environmental oxidation/corrosion banding close to initiation point (b) Back scattered electron (BSE) image of environmental oxidation/corrosion banding (c) SE image of environmental oxidation/corrosion banding (d) SE image of {1 1 1} fatigue striations prior to mechanical overload located on {1 1 1} facets.

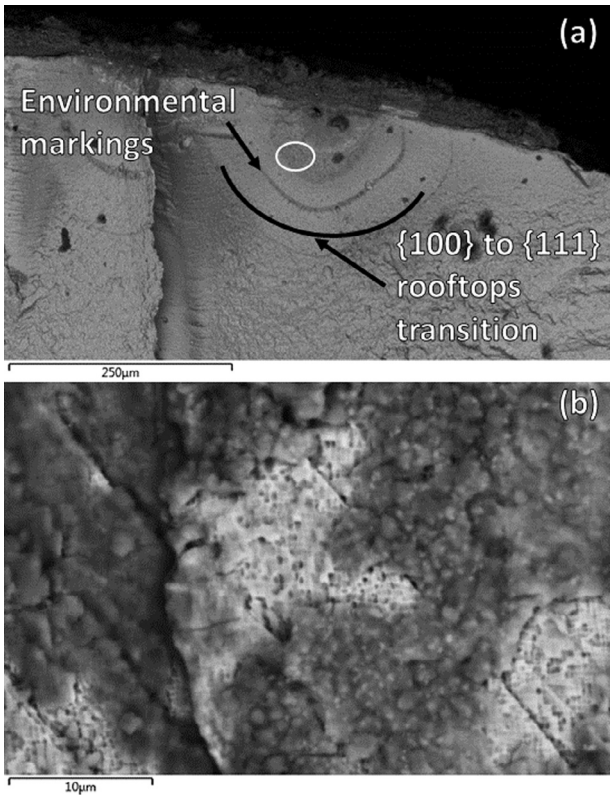


**Fig. 9.** BSE, SEM images of an 800 MPa , 5 µg/cm$^2$/h, 1-1-1-1 specimen (a) Fracture face showing transition between {1 0 0} and {1 1 1} [13] (b) Higher magnification of circled location in image (a) showing corrosion product build up on fracture surface.

analysing the crack length at which the $K_{TH}$ is exceeded, suggests that it is overcome at a length of around 114 µm for a plain specimen geometry loaded at 800 MPa uniaxial. This is of a similar magnitude to the measured values for {1 0 0} to {1 1 1} rooftop transition presented in Table 2, supporting this theory.

It is proposed that this transition in fracture face morphology is due to stage 1 crack initiation being associated to the time dependant, static-load driven crack growth. This accelerated stage 1 initiation has been observed to take the form of {1 0 0} crystallographic propagation, due to preferential γ′ corrosion attack at the crack tip [13]. However when stage 2 propagation is reached, propagation results from fatigue driven shear slip contributions in the crystallographic octahedral ⟨1 1 1⟩ directions.

## 5. Conclusions

- The introduction of a 60 s dwell period reduced the fatigue life of single crystal superalloy CMSX-4 when acting in combination with type II hot corrosion. Considering previous research into static stress cracking combined with type II corrosion, it was suggested that cracks could additionally propagate during the dwell period most notably aiding fatigue crack nucleation and initiation. Fatigue cracks demonstrated consistent surface initiation when exposed to a type II hot corrosion environment.
- It was found that 60 s dwell tests required a relatively longer test duration to fail than comparative 1 s dwell tests. It was proposed that this was due to dwell enhancing the fatigue crack nucleation and initiation, however when cracks exceeded the fatigue threshold $K_{TH}$ and entered stage 2 propagation, loading frequency and ΔK were the critical drivers determining crack propagation rates.
- The introduction of a 60 s dwell had the effect of increasing the number of {1 0 0} crack initiations particularly at lower stresses. This is theorised to be due to crack tip blunting due to oxidation and static stress cracking being less sensitive to stress intensity/concentration.

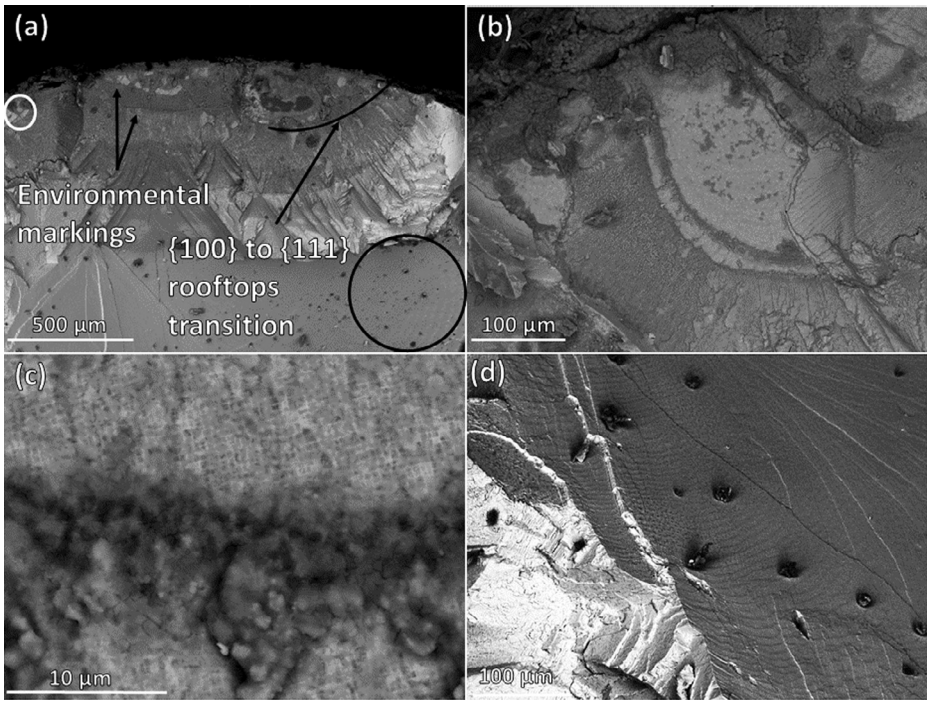


**Fig. 10.** SE SEM images of fracture face of specimen exposed to 800 MPa, 1-60-1-1, 5 µg/cm$^2$/h deposit flux (a) environmentally induced oxidation/corrosion markings and {1 0 0} to {1 1 1} transitioning (b) & (c) semi-circular oxide banding taken from white circled location in image (a) (d) fatigue striations taken from black circled location in image (a).

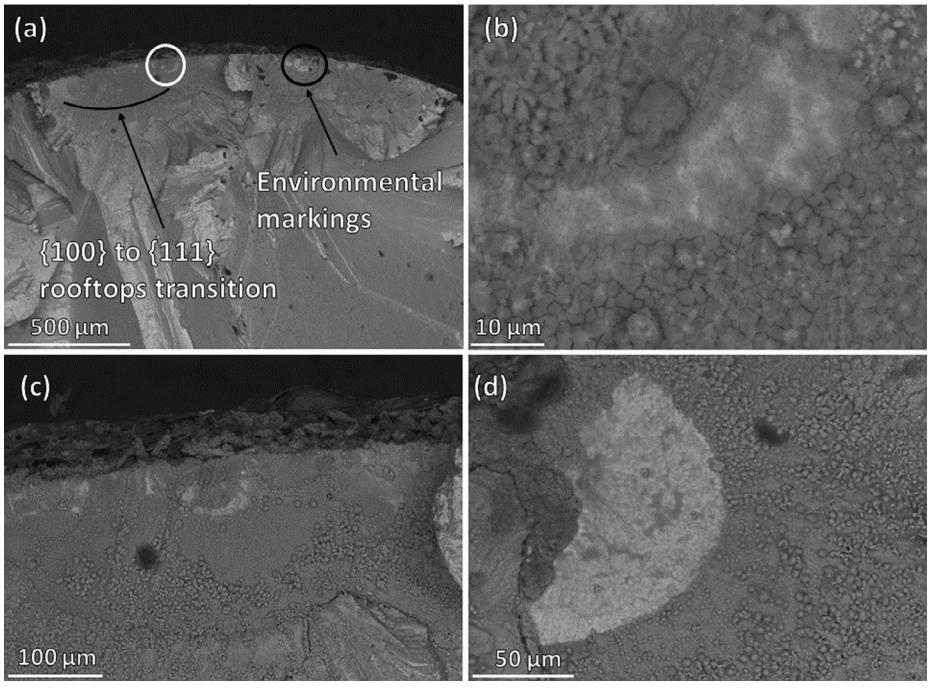


**Fig. 11.** SE SEM images of fracture face from a specimen exposed to 850 MPa, 1-60-1-1, 5 µg/cm$^2$/h deposit flux (a) environmentally induced oxidation/corrosion banding and {1 0 0} to {1 1 1} transitioning (b) & (c) semi-circular oxide banding taken from white location (d) shell shaped feature in the oxide scale taken from the black location.

**Table 3**
Environmental {0 0 1} spacing and fracture face analysis for 5 µg/cm$^2$/h flux.

| Stress (MPa) | Dwell time (s) | Number of {1 0 0} initiations over fracture face | Oxidation banding spacing (µm) | {1 0 0} to {1 1 1} transition length (µm) |
|---|---|---|---|---|
| 800 | 60 | 8 | 150–180 | 150–200 |
| 850 | 60 | 4 | 185–250 | 100–150 |
| 800 | 1 | 1 | 15–20 | 150–200 |

- Analysis of fracture faces suggests that the crack propagation mechanism propagates in a start/stop fashion. This maybe a result of a time-dependant corrosion embrittlement or crack tip oxidation.
- A correlation in the transition of fracture morphology from {1 0 0} to {1 1 1} rooftops with the $K_{TH}$ being exceeded was observed. This suggests corrosion has an influence in the crack propagation plane.
- Further research to confirm the nature of crack growth and determine crack growth rates under type II corrosion fatigue conditions is needed in order to account for its effects when designing GT components.

## Acknowledgements

The authors acknowledge the support of the Engineering and Physical Research Council (EPSRC) for their support for the project – Flexible and Efficient Power Plant: Flex-E-Plant (Grant number: EP/K021095/1). They also thank the following partners for their the valuable contributions: GE Energy, Doosan Babcock Limited, Centrica plc., EDF Energy (West Burton Power) Limited., Uniper Technologies Limited, Goodwin Steel Castings Limited, NPL Management Limited, R-MC Power Recovery Limited., RWE Generation UK plc., Scottish and Southern Energy (SSE) plc., Siemens Industrial Turbomachinery, and TWI Limited.

Data underlying this paper can be accessed at https://doi.org/10.17862/cranfield.rd.6845411.

## References

[1] UK Department of Energy and Climate Change. Updated energy and emissions projections 2013. Energy White Pap., vol. 947, no. November; 2008. p. 1–51.
[2] UNFCCC. Paris agreement. Conf. Parties its twenty-first Sess., no. December; 2015. p. 32.
[3] Sikorska PE. The need for legal regulation of global emissions from the aviation industry in the context of emerging aerospace vehicles. Int Comp Jurisprud 2015;1(2):133–42.
[4] Lagow BW. Materials Selection in gas turbine engine design and the role of low thermal expansion materials. JOM 2016;68(11):2770–5.
[5] Caron P, Khan T. Evolution of Ni-based superalloys for single crystal gas turbine blade applications. Aerosp Sci Technol 1999;3(8):513–23.
[6] Sass V, Glatzel U, Feller-Kniepmeier M. Anisotropic creep properties of the nickel-base superalloy CMSX-4. Acta Mater 1996;44(5):1967–77.
[7] Moverare JJ, Johansson S, Reed RC. Deformation and damage mechanisms during thermal-mechanical fatigue of a single-crystal superalloy. Acta Mater 2009;57(7):2266–76.
[8] Cockings HL, Perkins KM, Dowd M. Influence of environmental factors on the corrosion-fatigue response of a nickel-based superalloy. Mater Sci Technol (United Kingdom) 2017;33(9):1048–55.
[9] Dewangan R, Patel J, Dubey J, Sen PK, Kumar Bohidar S. Gas turbines blades—a critical review of failure on first and second stages. Int J Mech Eng Rob Res 2015;4(1).
[10] Mahobia GS, et al. Effect of hot corrosion on low cycle fatigue behavior of superalloy IN718. Int J Fatigue 2014;59:272–81.
[11] Rosier H, Perkins K, Girling A, Leggett J, Gibson G. Factors affecting the corrosion fatigue life in nickel based superalloys for disc applications. In: MATEC web conf., vol. 14; 2014. p. 03001.
[12] Brooking L, Sumner J, Gray S, Simms NJ. Stress corrosion of Ni-based superalloys. Mater High Temp 2017;35(December):120–9.
[13] Brooking L, Sumner J, Gray S, Nicholls JR, Marchant G, Simms NJ. Effect of stress state and simultaneous hot corrosion on the crack propagation and fatigue life of single crystal superalloy CMSX-4. Int J Fatigue 2018.
[14] Shifler DA. Hot corrosion: a modification of reactants causing degradation. Mater High Temp 2018;35(1–3):225–35.
[15] Eliaz N, Shemesh G, Latanision RM. Hot corrosion in gas turbine components. Eng Fail Anal 2002;9(1):31–43.
[16] Sumner J, Encinas-Oropesa A, Simms NJ, Nicholls JR. Type II hot corrosion: kinetics studies of CMSX-4. Oxid Met 2013;80(5–6):553–63.
[17] Santoro GJ, Gokoglu SA, Kohl FJ, Stearns CA, Rosner DA. Deposition of $Na_2SO_4$ from salt-seeded combustion gases of a high velocity burner rig. AIME Metall Soc 1984:417–34.
[18] Birello F, Borello D, Venturini P, Rispoli F. Modelling of deposit mechanisms around the stator of a gas turbine. Aircr. Engine; Coal, Biomass Altern. Fuels; Cycle Innov., vol. 2, no. May 2016; 2013. p. V002T03A019.
[19] Tomeczek J, Palugniok H, Ochman JO. Modelling of deposits formation on heating tubes in pulverized coal boilers. Fuel 2004;83(2):213–21.
[20] Rengara B, Baba S, Okazaki M. Influence of crystal orientation on cyclic sliding friction and fretting fatigue behavior of single crystal Ni-base superalloys. In: Superalloys 2016: proceedings of the 13th international symposium on superalloys; 2016. p. 395–404.
[21] Sass V, Glatzel U, Feller-Kniepmeier M. Creep anisotropy in the monocrystalline nickel-base superalloy CMSX-4. In: Superalloys 1996 8th int. symp. superalloys; 1996. p. 283–90.
[22] Dowling NE. Mechanical behavior of materials. 4th ed. Boston, MA: Pearson; 2012.
[23] Joyce MR, Wu X, Reed PAS. The effect of environment and orientation on fatigue crack growth behaviour of CMSX-4 nickel base single crystal at 650 °C. Mater Lett 2004;58(1–2):99–103.
[24] Anderson TL. Fract Mech: Fundam Appl 2012;58:1.
[25] Pippan R. Dislocation emission a N D fatigue crack growth threshold, vol. 39, no. 3; 1990. p. 255–62.
[26] "Image-J." Oxford Instruments; 2017.
[27] Li YG, Nilkitsaranont P. Gas turbine performance prognostic for condition-based maintenance. Appl Energy 2009;86(10):2152–61.
[28] Mao SX, Evans AG. The influence of blunting on crack growth oxide/metal interfaces. Acta Metall 1997;45(10):4263–70.